ACS Photonics

pubs.acs.org/journal/apchd5

Article

Enhancing Extended SWIR $Al_{0.3}InAsSb$ PIN Photodetectors with All-Dielectric Amorphous Germanium Photon-Capturing Gratings

Dongxia Wei, Adam A. Dadey, J. Andrew McArthur, Seth R. Bank, and Joe Charles Campbell*

Cite This: *ACS Photonics* 2024, 11, 484−488

Read Online

ACCESS | Metrics & More | Article Recommendations | Supporting Information

ABSTRACT: The extended short-wavelength infrared (eSWIR) spectrum, spanning from 1.9 to 2.2 μm, plays a pivotal role in many civil and military applications. Consequently, there is a consistent demand for high-performance eSWIR photonic devices, such as photodetectors, to drive technological advancements This study explores improving the absorption efficiency of $Al_{0.3}InAsSb$ PIN photodetectors at the critical 2 μm wavelength. Our research highlights the potential of amorphous germanium (a-Ge), a transparent dielectric material with a high refractive index, in enhancing the performance of eSWIR photodetectors. We report an 113% experimental improvement in quantum efficiency for a digital alloy $Al_{0.3}InAsSb$ PIN photodetector by employing an all-dielectric photon-capturing structure composed of one-dimensional (1D) a-Ge gratings. Our simulations reveal that the 1D a-Ge grating effectively confines electromagnetic fields within the absorption layer and significantly reduces reflection.

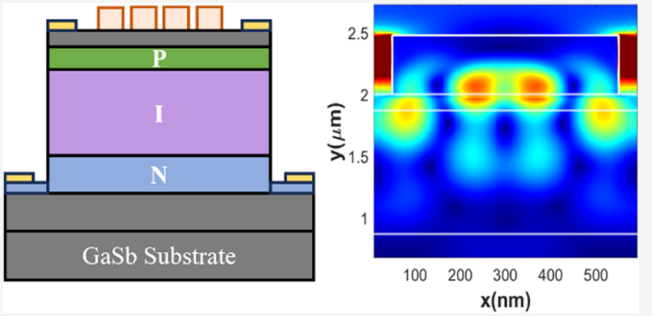

KEYWORDS: *extended SWIR, PIN photodetector, photon-capturing, germanium grating, quantum efficiency*

INTRODUCTION

The extended short-wavelength infrared (eSWIR) (1.9−2.2 μm) range holds significant importance in various civil and military applications, encompassing surveillance,[1,2] night vision,[3] trace molecule sensing,[1,4] weather forecasting,[5] and environmental monitoring.[6] Consequently, the demand for high-performance eSWIR photonic devices, specifically eSWIR photodetectors, has remained consistently high for several decades.

Digital alloy $Al_xIn_{1-x}As_ySb_{1-y}$ has been demonstrated as a tunable material system that can be used to create eSWIR separate absorption, charge and multiplication (SACM) avalanche photodiodes (APDs).[7−9] Previously, we have reported light absorption enhancement in SACM digital alloy $Al_{0.3}$ InAsSb APDs operating at 2 μm.[10,11] This enhancement was achieved by implementing a photon-trapping structure created by using gold (Au). Other papers also report using Au nanostructure to enhance the field of photodetector through plasmonic effect.[12−14] However, gold, being a noble metal, presents challenges due to its cost and the complexity of fabricating dense nanostructures with high aspect ratios by using conventional lift-off techniques. In addition, the loss of the nature of metal nanostructures limits their application. One way to circumvent this problem is to replace the lossy metal with dielectrics with a high refractive index and low absorption coefficient.[15,16]

Germanium (Ge), on the other hand, stands out as a transparent dielectric material in the eSWIR spectrum, boasting a high refractive index of 4.1. This makes it ideal for crafting all-dielectric optical nanostructures applicable to various scenarios, including grating couplers,[17,18] waveguides,[19] and metasurfaces.[20,21] Here, we report on using amorphous germanium (a-Ge), which shares optical properties similar to those of crystalline Ge in the eSWIR spectrum to enhance the light absorption of eSWIR photodetectors.

This study achieves a significant improvement in external quantum efficiency (EQE) at 2 μm for a digital alloy $Al_{0.3}$ InAsSb ($E_g \approx 0.58$ eV) PIN photodetector. This improvement is achieved by implementing an all-dielectric photon-capturing structure composed of one-dimensional (1D) a-Ge gratings. Compared to their metallic counterparts, a-Ge-based structures offer distinct advantages, including cost-effectiveness and ease of nanofabrication through standard dry etching techniques. This allows for the creation of high-density nanostructures with substantial aspect ratios.

DESIGN

Figure 1a shows the structure of the $Al_{0.3}InAsSb$ PIN photodetector and the design of the 1D a-Ge grating. The

Received: September 14, 2023
Revised: December 27, 2023
Accepted: December 27, 2023
Published: January 9, 2024

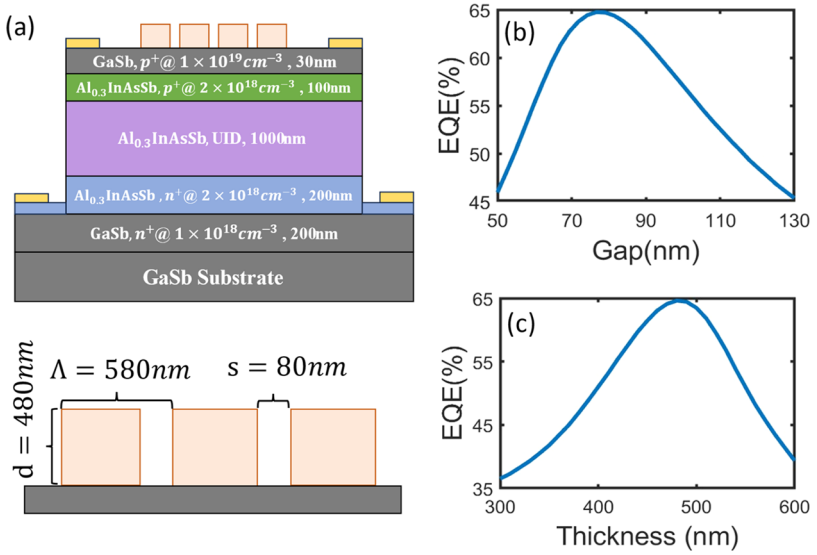

Figure 1. (a) Structure of the $Al_{0.3}InAsSb$ photodetector and the simulated optimal a-Ge grating; (b) simulated quantum efficiency as a function of the gap width of gratings; and (c) simulated quantum efficiency as a function of a-Ge thickness.

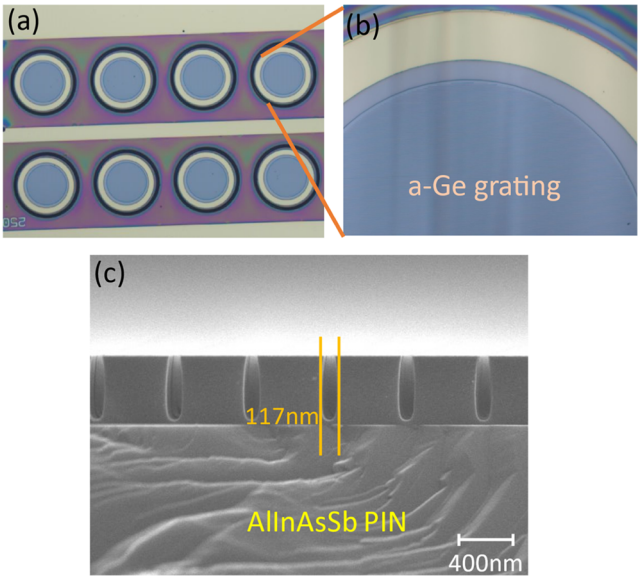

Figure 2. (a) Top-down view of fabricated mesa devices under an optical microscope; (b) magnified area to show the a-Ge grating under an optical microscope; and (c) cross-sectional SEM image of the cleaved 1D a-Ge grating.

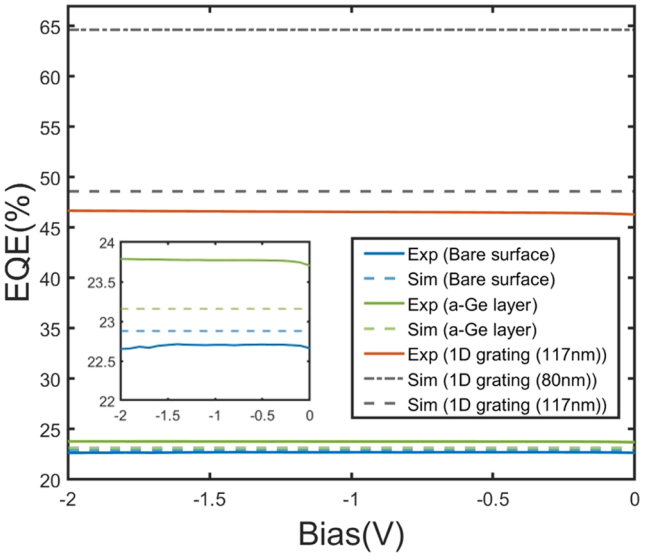

Figure 3. Measured and simulated quantum efficiencies as a function of reverse bias. The inset zoom in the figure for EQE from 22 to 24%.

PIN photodetector structure comprises a 100 nm highly p-doped layer, a 1 μm intrinsic layer, and a 200 nm highly n-doped layer. The structure is capped with a highly doped 30 nm GaSb cap layer. Figure 1b,c presents the simulated EQE for a 2 μm wavelength as a function of the a-Ge thickness and trench spacing for incident light with an electric field polarized perpendicular to the grating. These simulations were conducted using the ANSYS Lumerical FDTD module. The refractive index and the extinction coefficient of $Al_{0.3}InAsSb$ were determined through ellipsometry measurements and fitting of the simulated data to experimental EQE measurements. The optimized structural parameters were identified as follows: a period of 580 nm, a thickness of 480 nm, and a spacing of 80 nm. The EQE of the bare surface sample, as will be discussed later, was measured as approximately 22.6%. In contrast, the simulated EQE for the optimized structure reached around 65%, nearly tripling the performance of the bare surface configuration.

EXPERIMENTS

The $Al_{0.3}InAsSb$ ($E_g \approx 0.58$ eV) digital alloy PIN structure on a GaSb substrate was grown by molecular beam epitaxy on a GaSb substrate. The amorphous a-Ge layer was deposited by e-beam evaporation. A dry etch mask for the 1D grating pattern was then defined using a PMMA 950 K A4 resist and E-beam lithography. After developing the e-beam resist in a mixed solution of IPA and water, the specified pattern was dry-etched by inductively coupled plasma reactive ion etching (ICP-RIE). The thickness, period, and spacing of the 1D a-Ge gratings were designed to be 480, 580, and 80 nm, respectively, to optimize the EQE based on the simulation results discussed above. The cross-sectional profile of the grating was imaged using a scanning electron microscope (SEM). Figure 2c shows

https://doi.org/10.1021/acsphotonics.3c01317
ACS Photonics 2024, 11, 484−488

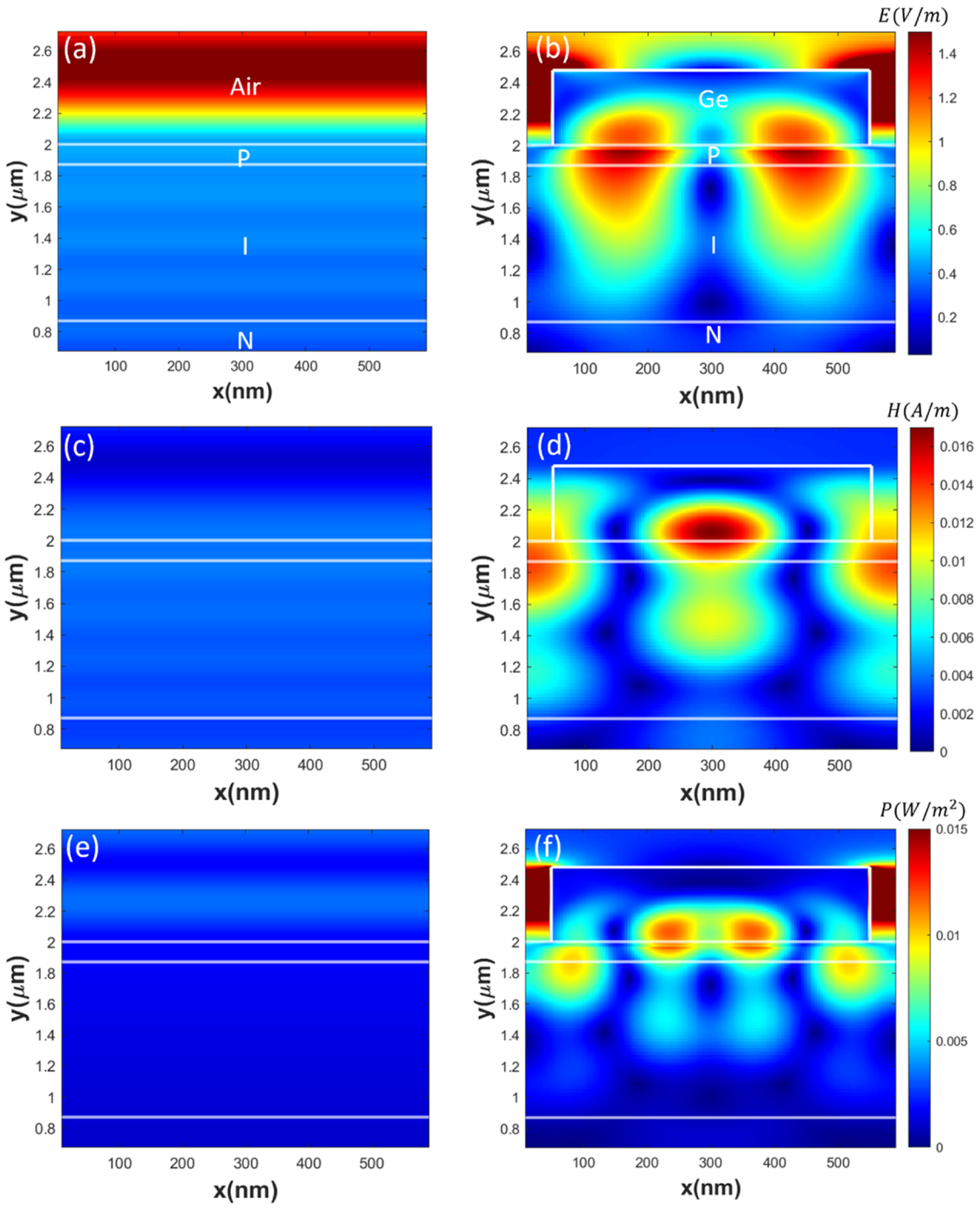

Figure 4. Simulated electric field (a, b), magnetic field (c, d), and Poynting vector distribution (e, f) of the sample with a bare surface (left) and grating (right). The grating period, thickness, and gap are 580, 480, and 80 nm, respectively.

that the grating sidewall is mostly vertical but has a slight curvature. Changing the ratio of the component etching gases might further improve the etch profile. The top opening of the gap is around 80 nm, but the largest gap is measured to be about 117 nm. After etching the grating, the a-Ge layer not on the device's top area was removed using the same dry etch process. After fabrication of the a-Ge grating, the photodetector was fabricated by utilizing a mesa wet etch process. The top and bottom contacts were then deposited by evaporating 10/90 nm of Ti/Au and a subsequent lift-off process (Figure 2a,b).

To measure the EQE, a 2 μm semiconductor laser was focused on the top opening of the sample at a normal incidence. A 3-paddle fiber polarizer was used to adjust the polarization of the laser such that the incident electric field is perpendicular to the grating. The dark current (I_d) and the total current (I_{total}) were measured using a Keithley 2400 Sourcemeter. A Thorlabs optical power and energy meter measured the output power (P) of the laser. The EQE of the sample was calculated from the relationship between the responsivity and the EQE as the following equation

https://doi.org/10.1021/acsphotonics.3c01317
ACS Photonics 2024, 11, 484−488

$$\mathrm{EQE} = \frac{I_{\mathrm{total}} - I_{\mathrm{d}}}{P} \times \frac{hc}{\lambda q} \quad (1)$$

where h is Planck's constant, c is the speed of light, q is the electron charge, and λ is the wavelength of the incident light, which is equal to 2 μm.

RESULTS AND DISCUSSION

Figure 3 compares the experimental and simulated EQE of devices with a bare surface, an unpatterned a-Ge layer, and a 1D a-Ge grating. Notably, the EQE remains relatively stable as the reverse bias increases. This stability arises from minimal changes in the width of the depletion region when both the p-region and the n-region are highly doped. The EQE of the sample with a bare surface is around 22.6%, while that of the sample with the unpatterned a-Ge layer is slightly higher, at 23.7%. In contrast, the sample incorporating the 1D a-Ge gratings achieves an EQE of 47%, more than double that of the bare surface.

The figure also depicts simulated EQE values for a-Ge gratings with gap widths of 117 nm and the optimal 80 nm. Notably, the measured EQE aligns closely with the 117 nm wide gap simulation results. While other factors, such as grating sidewall roughness, interface defects, and imperfect stitch boundary from e-beam lithography, may influence the EQE, the gap size between gratings plays a pivotal role in the performance of the photon-capturing structure. Moreover, they pose particular challenges during fabrication. We also conducted specific detectivity measurements for all samples (Figure S1). The specific detectivity of the sample with 1D a-Ge grating is approximately $5.6 \times 10^{10}(\mathrm{cm}\cdot\sqrt{\mathrm{Hz}}/\mathrm{W})$ at −0.05 V, exhibiting a 68% improvement in comparison to the sample with a bare surface, which showed a specific detectivity of $3.3 \times 10^{10}(\mathrm{cm}\cdot\sqrt{\mathrm{Hz}}/\mathrm{W})$.

To delve into the absorption enhancement mechanism of 1D a-Ge gratings, Figure 4 illustrates the distribution of electric fields, magnetic fields, and Poynting vectors within the structure. Compared to the bare surface sample, the a-Ge grating significantly confines the electromagnetic field within the absorber layer rather than allowing it to pass through. Previous studies suggest that this enhancement primarily results from diffraction, as light interacts with the gratings. The diffraction effect is intricate, involving both constructive interference within the structure, which strengthens the field, and destructive interference, which nearly eliminates direct reflection.[22] According to FDTD simulations, the bare surface sample exhibits a reflection of approximately 30%, whereas the sample with the a-Ge grating achieves a remarkably low reflection of only 0.66%. Therefore, the a-Ge grating effectively serves as an antireflection layer. This phenomenon can be further explained by treating dielectric grating surrounded by air as waveguides.[23] As light travels through the waveguide, a few waveguide modes are excited. Due to the index mismatch, these modes will propagate downward the grating and then reflect back at the interface of the grating and the bottom substrate. During this process, the modes will couple each other and interfere with the incident light. To cancel the reflection, the grating structure is designed such that the spatial mode in the grating and incident wave achieves a complete impedance match at the input plane, which is the case for the 1D a-Ge grating reported in this paper.

Using an a-Ge grating to enhance the photodetector quantum efficiency presents distinct advantages. Compared to directly etching the photodetector into microstructures to enhance light absorption,[24,25] placing an a-Ge grating on top does not introduce a significant additional surface leakage current that would increase the dark current (Figure S2). Furthermore, when compared to the utilization of metal nanostructures,[11−14] an all-dielectric a-Ge grating avoids substantial optical loss. It is cost-effective and much easier to fabricate through plasmonic dry etching.

CONCLUSIONS

In this study, we have demonstrated a significant enhancement in the absorption efficiency of $Al_{0.3}$ InAsSb PIN photodetectors at 2 μm by integrating 1D a-Ge photon-capturing gratings. These findings underscore the potential of a-Ge as an effective and cost-efficient material for improving light absorption in eSWIR photonic devices.

It is worth noting that the current 1D a-Ge grating exhibits polarization-dependent behavior (Figure S3), enhancing light with an electric field perpendicular to the grating direction. Looking ahead, future work will progress toward the development of 2D gratings that are insensitive to polarization. This advancement holds the promise of broadening the scope of applications for a-Ge, further solidifying its role as an economical and high-performance material for enhancing light absorption in eSWIR photonic devices.

ASSOCIATED CONTENT

Supporting Information

The Supporting Information is available free of charge at https://pubs.acs.org/doi/10.1021/acsphotonics.3c01317.

S1: Specific detectivity; S2: dark current; and S3: polarization-dependent behavior (PDF)

AUTHOR INFORMATION

Corresponding Author

Joe Charles Campbell − *Department of Electrical and Computer Engineering, University of Virginia, Charlottesville, Virginia 22904, United States;* orcid.org/0000-0001-6812-7647; Email: jcc7s@virginia.edu

Authors

Dongxia Wei − *Department of Electrical and Computer Engineering, University of Virginia, Charlottesville, Virginia 22904, United States*

Adam A. Dadey − *Department of Electrical and Computer Engineering, University of Virginia, Charlottesville, Virginia 22904, United States;* orcid.org/0000-0002-1018-3651

J. Andrew McArthur − *Microelectronics Research Center, University of Texas, Austin, Texas 78758, United States*

Seth R. Bank − *Microelectronics Research Center, University of Texas, Austin, Texas 78758, United States;* orcid.org/0000-0002-5682-0126

Complete contact information is available at: https://pubs.acs.org/10.1021/acsphotonics.3c01317

Funding

This work was funded by the National Science Foundation under Contract 1838435.

Notes

The authors declare no competing financial interest.

■ ACKNOWLEDGMENTS

The authors would like to express their sincere gratitude to Daniel Herrera for his invaluable assistance and support during the preparation of this paper.

■ REFERENCES

(1) Willer, U.; Saraji, M.; Khorsandi, A.; Geiser, P.; Schade, W. Near- and Mid-Infrared Laser Monitoring of Industrial Processes, Environment and Security Applications. *Opt Lasers Eng.* **2006**, *44* (7), 699−710.

(2) Fossi, A. P.; Ferrec, Y.; Roux, N.; D'almeida, O.; Guerineau, N.; Sauer, H. Miniature and Cooled Hyperspectral Camera for Outdoor Surveillance Applications in the Mid-Infrared. *Opt. Lett.* **2016**, *41* (9), 1901−1904.

(3) Rowan-Robinson, M. *Night Vision: Exploring the Infrared Universe*; Cambridge University Press, 2013.

(4) Tittel, F. K.; Richter, D.; Fried, A. Mid-Infrared Laser Applications in Spectroscopy. In *Solid-State Mid-Infrared Laser Sources*; Sorokina, I. T.; Vodopyanov, K. L., Eds.; Springer: Berlin, 2003; pp 458−529.

(5) Hu, X. Q.; Lu, N. M.; Niu, T.; Zhang, P. Operational Retrieval of Asian Sand and Dust Storm from FY-2C Geostationary Meteorological Satellite and Its Application to Real Time Forecast in Asia. *Atmos. Chem. Phys.* **2008**, *8* (6), 1649−1659.

(6) Mizaikoff, B. Waveguide-Enhanced Mid-Infrared Chem/Bio Sensors. *Chem. Soc. Rev.* **2013**, *42* (22), 8683−8699.

(7) Jones, A. H.; March, S. D.; Bank, S. R.; Campbell, J. C. Low-Noise High-Temperature AlInAsSb/GaSb Avalanche Photodiodes for 2-μm Applications. *Nat. Photonics* **2020**, *14* (9), 559−563.

(8) Jones, A. H.; March, S. D.; Dadey, A. A.; Muhowski, A. J.; Bank, S. R.; Campbell, J. C. AlInAsSb Separate Absorption, Charge, and Multiplication Avalanche Photodiodes for Mid-Infrared Detection. *IEEE J. Quantum Electron.* **2022**, *58* (4), No. 4500306, DOI: 10.1109/JQE.2022.3149532.

(9) McArthur, J. A.; Dadey, A. A.; March, S. D.; Jones, A. H.; Xue, X.; Salas, R.; Campbell, J. C.; Bank, S. R. Demonstration of the AlInAsSb Cascaded Multiplier Avalanche Photodiode. *Appl. Phys. Lett.* **2023**, *123* (4), No. 041106.

(10) Chen, D.; Sun, K.; Jones, A. H.; Campbell, J. C. Efficient Absorption Enhancement Approaches for AlInAsSb Avalanche Photodiodes for 2-μm Applications. *Opt. Express* **2020**, *28* (17), 24379−24388.

(11) Chen, D.; March, S. D.; Jones, A. H.; Shen, Y.; Dadey, A. A.; Sun, K.; McArthur, J. A.; Skipper, A. M.; Xue, X.; Guo, B.; Bai, J.; Bank, S. R.; Campbell, J. C. Photon-Trapping-Enhanced Avalanche Photodiodes for Mid-Infrared Applications. *Nat. Photonics* **2023**, *17* (7), 594−600.

(12) Yadav, S. N. S.; Chen, P.-L.; Liu, C. H.; Yen, T.-J. Plasmonic Metasurface Integrated Black Phosphorus-Based Mid-Infrared Photodetector with High Responsivity and Speed. *Adv. Mater. Interfaces* **2023**, *10* (10), No. 2202403.

(13) Tong, J.; Tobing, L. Y. M.; Qiu, S.; Zhang, D. H.; Unil Perera, A. G. Room Temperature Plasmon-Enhanced InAs0.91Sb0.09-Based Heterojunction n-i-p Mid-Wave Infrared Photodetector. *Appl. Phys. Lett.* **2018**, *113* (1), No. 011110.

(14) Nolde, J. A.; Kim, M.; Kim, C. S.; Jackson, E. M.; Ellis, C. T.; Abell, J.; Glembocki, O. J.; Canedy, C. L.; Tischler, J. G.; Vurgaftman, I.; Meyer, J. R.; Aifer, E. H. Resonant Quantum Efficiency Enhancement of Midwave Infrared NBn Photodetectors Using One-Dimensional Plasmonic Gratings. *Appl. Phys. Lett.* **2015**, *106* (26), No. 261109.

(15) Genevet, P.; Capasso, F.; Aieta, F.; Khorasaninejad, M.; Devlin, R. Recent Advances in Planar Optics: From Plasmonic to Dielectric Metasurfaces. *Optica* **2017**, *4* (1), 139−152.

(16) Overvig, A. C.; Shrestha, S.; Malek, S. C.; Lu, M.; Stein, A.; Zheng, C.; Yu, N. Dielectric Metasurfaces for Complete and Independent Control of the Optical Amplitude and Phase. *Light: Sci. Appl.* **2019**, *8* (1), 92.

(17) Alonso-Ramos, C.; Nedeljkovic, M.; Benedikovic, D.; Penadés, J. S.; Littlejohns, C. G.; Khokhar, A. Z.; Pérez-Galacho, D.; Vivien, L.; Cheben, P.; Mashanovich, G. Z. Germanium-on-Silicon Mid-Infrared Grating Couplers with Low-Reflectivity Inverse Taper Excitation. *Opt. Lett.* **2016**, *41* (18), 4324−4327.

(18) Yang, S.; Zhang, Y.; Baehr-Jones, T.; Hochberg, M. High Efficiency Germanium-Assisted Grating Coupler. *Opt. Express* **2014**, *22* (25), 30607−30612.

(19) Nedeljkovic, M.; Penades, J. S.; Mittal, V.; Murugan, G. S.; Khokhar, A. Z.; Littlejohns, C.; Carpenter, L. G.; Gawith, C. B. E.; Wilkinson, J. S.; Mashanovich, G. Z. Germanium-on-Silicon Waveguides Operating at Mid-Infrared Wavelengths up to 8.5 μm. *Opt. Express* **2017**, *25* (22), 27431−27441.

(20) Zhou, Z.-X.; Ye, M.-J.; Yu, M.-W.; Yang, J.-H.; Su, K.-L.; Yang, C.-C.; Lin, C.-Y.; Babicheva, V. E.; Timofeev, I. V.; Chen, K.-P. Germanium Metasurfaces with Lattice Kerker Effect in Near-Infrared Photodetectors. *ACS Nano* **2022**, *16* (4), 5994−6001.

(21) Masoudian Saadabad, R.; Huang, L.; Miroshnichenko, A. E. Polarization-Independent Perfect Absorber Enabled by Quasibound States in the Continuum. *Phys. Rev. B* **2021**, *104* (23), No. 235405.

(22) Optical Coupling. In *Quantum Well Infrared Photodetectors: Physics and Applications*; Schneider, H.; Liu, H. C., Eds.; Springer: Berlin, 2007; pp 97−105.

(23) Chang-Hasnain, C. J.; Yang, W. High-Contrast Gratings for Integrated Optoelectronics. *Adv. Opt. Photonics* **2012**, *4* (3), 379−440.

(24) Zhou, H.; Xu, S.; Lin, Y.; Huang, Y.-C.; Son, B.; Chen, Q.; Guo, X.; Lee, K. H.; Goh, S. C.-K.; Gong, X.; Tan, C. S. High-Efficiency GeSn/Ge Multiple-Quantum-Well Photodetectors with Photon-Trapping Microstructures Operating at 2 μm. *Opt. Express* **2020**, *28* (7), 10280−10293.

(25) Suo, F.; Tong, J.; Zhang, D. H. Photon-Trapping Array for Enhanced Midwave Infrared Photoresponse. *J. Phys. D: Appl. Phys.* **2021**, *54* (50), No. 505105.